

Quantum droplet states of a binary magnetic gas

Joseph C. Smith, D. Baillie, and P. B. Blakie

*Dodd-Walls Centre for Photonic and Quantum Technologies, New Zealand and
Department of Physics, University of Otago, Dunedin 9016, New Zealand*

(Dated: July 2, 2020)

Quantum droplets can emerge in bosonic binary magnetic gases (BMGs) from the interplay of short- and long-ranged interactions, and quantum fluctuations. We develop an extended meanfield theory for this system and use it to predict equilibrium and dynamical properties of BMG droplets. We present a phase diagram and characterize miscible and immiscible droplet states. We also show that a single component self-bound droplet can be used to bind another magnetic component which is not in the droplet regime. Our results should be realizable in experiments with mixtures of highly-magnetic lanthanide atoms.

Introduction - Quantum droplets are a dilute liquid-like state of an ultra-cold atomic gas that occurs when collapse-inducing attractive two-body interactions are balanced by a repulsive term with a higher-order dependence on the density [1]. Experimental studies over the past four years have produced quantum droplets in two different bosonic systems in which the collapse is stabilized by quantum fluctuations¹: (i) Binary mixtures of atoms with an attractive interspecies interaction [2]. These droplets have been prepared with mixtures of potassium spin states [3, 4], and with a heteronuclear potassium-rubidium [5] mixture. (ii) Single-component systems of highly magnetic atoms in the regime where the magnetic dipole-dipole interaction (DDI) dominates over the contact interaction. Gases of dysprosium (Dy) [6] and erbium (Er) [7] atoms have been used to prepare these droplets.

Here we consider a new class of quantum droplet formed in a BMG, i.e. a two-component bosonic gas, where the atoms of each component have a large magnetic moment. In this system each component can independently form a droplet, but together the components have an array of interactions that lead to a multi-component droplet with unique features. Critically, interactions can favour the droplet being either in a miscible or immiscible phase. In the latter case the long-ranged DDIs play an important role in organising the phase-separated parts of the droplet. Such multi-component physics is absent from (non-magnetic) binary mixtures, for which the interspecies attraction only allows droplets to form in the miscible regime, where it effectively behaves as a single component system (see [2]). Motivation for understanding this new system comes from recent experimental progress with BMGs [8], where binary Bose-Einstein condensates with five different Er-Dy isotope combinations have been produced.

Formalism - We consider a zero temperature gas of two bosonic atoms with a large magnetic moment μ_i^m ($i = 1, 2$), polarized along the z axis. In this work we assume both species have the same mass m , which well-approximates any mixture of Er and Dy isotopes. The stationary states of species i are described by the extended GPE $\mathcal{L}_i \psi_i = \mu_i \psi_i$, where

$$\mathcal{L}_i = h_{\text{sp}} + \sum_j g_{ij} n_j + \sum_j g_{ij}^{\text{dd}} \Phi_j(\mathbf{x}) + \Delta \mu_i, \quad (1)$$

and μ_i is the chemical potential of species i , used to fix the number of atoms $N_i = \int d\mathbf{x} |\psi_i|^2$. Here $h_{\text{sp}} = -\frac{\hbar^2 \nabla^2}{2m} + V(\mathbf{x})$ is the single-particle Hamiltonian, where $V(\mathbf{x})$ represents any external potential. The short-ranged two-body interaction coupling constants are $g_{ij} = 4\pi\hbar^2 a_{ij}/m$, where a_{ij} is the s -wave scattering length between species i and j . The long-ranged DDIs are described by $\Phi_i(\mathbf{x}) = \int d\mathbf{x}' f^{\text{dd}}(\mathbf{x} - \mathbf{x}') |\psi_i(\mathbf{x}')|^2$, where $f^{\text{dd}}(\mathbf{r}) = \frac{3}{4\pi r^3} (1 - 3\cos^2\theta)$, with the coupling constant $g_{ij}^{\text{dd}} = 4\pi\hbar^2 a_{ij}^{\text{dd}}/m$ and $a_{ij}^{\text{dd}} = m\mu_0 \mu_i^m \mu_j^m / 12\pi\hbar^2$ being the dipole length.

The quantum fluctuation effects included in the eGPE are described by the terms $\Delta \mu_i$, derived by extending the formalism of Ref. [2] to include DDIs. For a uniform (and equal mass) dipolar mixture of component density n_i the quantum fluctuations contribute an energy density of $\mathcal{E}_{\text{QF}} = \frac{\sqrt{2}m^{3/2}}{15\pi^2\hbar^3} \sum_{\pm} \int_0^{\pi/2} d\theta_k \sin\theta_k I_{E\pm}^{5/2}$ where

$$I_{E\pm} = n_1 \tilde{U}_{11} + n_2 \tilde{U}_{22} \pm \sqrt{\delta_1^2 + 4\tilde{U}_{12}^2 n_1 n_2}, \quad (2)$$

with $\delta_1 = n_1 \tilde{U}_{11} - n_2 \tilde{U}_{22}$, and $\tilde{U}_{ij}(\mathbf{k}) = g_{ij} + g_{ij}^{\text{dd}} (\cos^2\theta_k - \frac{1}{3})$ being the Fourier transform of the total interaction potential. From this we derive the chemical potential correction as $\Delta \mu_i = \partial_{n_i} \mathcal{E}_{\text{QF}} = \frac{m^{3/2}}{3\sqrt{2}\pi^2\hbar^3} \sum_{\pm} \int_0^{\pi/2} d\theta_k \sin\theta_k I_{i\pm}$, where

$$I_{i\pm} = \left(\tilde{U}_{11} \pm \frac{\delta_1 \tilde{U}_{11} + 2\tilde{U}_{12}^2 n_2}{\sqrt{\delta_1^2 + 4\tilde{U}_{12}^2 n_1 n_2}} \right) I_{E\pm}^{3/2}. \quad (3)$$

We omit writing the similar expression for I_2 . This theory will provide a good description in the dilute regime, which is well-satisfied in ultra-cold atomic experiments. To employ this result in the inhomogeneous situation of Eq. (1) we make the local density approximation and set $n_i = |\psi_i(\mathbf{x})|^2$. In using these expressions we ignore the small imaginary part of $\Delta \mu_i$, consistent with previous treatments [2, 6] (also see [9]).

Quantum droplets in the balanced BMG - First we consider a balanced mixture with equal intra-species interactions and particle numbers in each component (i.e. $a_{11} = a_{22}$, $a_{11}^{\text{dd}} = a_{22}^{\text{dd}}$, and $N_1 = N_2$). In the regime where both components are miscible and take the same shape (i.e. $\psi_1 = \psi_2$) the eGPE can be reduced to an effective single component problem which we refer to as the same shape approximation (SSA):

$$\mathcal{L}_i^{\text{SSA}} = h_{\text{sp}} + g_{\text{eff}} n_i + g_{\text{eff}}^{\text{dd}} \Phi_i + \gamma_{\text{QF}} n_i^{3/2}, \quad (4)$$

¹ Here the energy of the two-body interactions and quantum fluctuations scale with the density n as $\mathcal{E}_{\text{B}} \sim n^2$ and $\mathcal{E}_{\text{QF}} \sim n^{5/2}$, respectively.

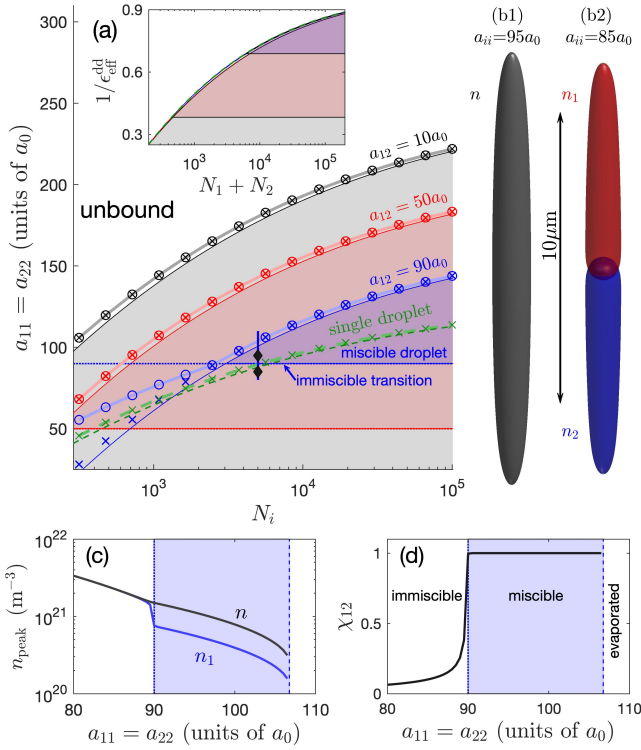


FIG. 1. Free-space droplets and miscibility in a balanced BMG. (a) Phase diagram as a function of atom number and intra-species interactions for various a_{12} . BMG droplet binding predicted by variational theory (solid lines), eGPE (circles and thicker lines) and SSA eGPE (crosses). The immiscibility transition is at $a_{ii} = a_{12}$ (dotted horizontal lines) with shaded regions indicating where miscible self-bound droplets are predicted by variational theory. The self-binding boundary for a single-component system (green dashed lines and markers). Inset shows the variational results plotted as $1/\epsilon_{\text{eff}}^{\text{dd}}$ versus $N_1 + N_2$ (the single-droplet results as $a_{ii}/a_{ii}^{\text{dd}}$ versus N_i). eGPE droplet solutions in the (b1) miscible and (b2) immiscible regimes shown with a density isosurface at $2.5 \times 10^{20} \text{m}^{-3}$ for (b1) $n = n_1 + n_2$ (grey surface) and (b2) n_1 (red surface) and n_2 (blue surface). (c) The maximum of n_1 (blue line) and n (black line), and (d) the component overlap of the eGPE solution as a_{ii} is varied. The parameters for (b1), (b2) and the results in (c) and (d) are indicated in (a) by the diamonds and vertical line, respectively. Other parameters $a_{ii}^{\text{dd}} = 130.8a_0$, $m = 164u$, and in (b)-(d) $N_i = 5 \times 10^3$.

where we have set $g_{\text{eff}} \equiv g_{ii} + g_{12}$, and $g_{\text{eff}}^{\text{dd}} \equiv 2g_{ii}^{\text{dd}}$ as the effective two-body contact and dipolar coupling constants, respectively. Here the quantum fluctuations ($\Delta\mu_i$) depend on the density as $n_i^{3/2}$ with coefficient

$$\gamma_{\text{QF}} = \frac{2m^{3/2}}{3\pi^2\hbar^3} \left[(g_{ii} - g_{12})^{5/2} + (g_{\text{eff}}^{\text{dd}})^{5/2} \mathcal{M}_5(1/\epsilon_{\text{eff}}^{\text{dd}}) \right], \quad (5)$$

where $\epsilon_{\text{eff}}^{\text{dd}} \equiv g_{\text{eff}}^{\text{dd}}/g_{\text{eff}}$ and $\mathcal{M}_5(x) \equiv \text{Re} \int_0^1 du (x + 3u^2 - 1)^{5/2}$. The function \mathcal{M}_5 can be analytically evaluated² and

$${}^2 \mathcal{M}_5(x) = \frac{9+4x+11x^2}{16} \sqrt{2+x} - \frac{5(1-x)^3}{32\sqrt{3}} \left[2 \log(\sqrt{2+x} + \sqrt{3}) - \right.$$

has the following limits:

$$\begin{cases} (g_{\text{eff}}^{\text{dd}})^{5/2} \mathcal{M}_5(1/\epsilon_{\text{eff}}^{\text{dd}}) \rightarrow (g_{\text{eff}})^{5/2}, & g_{\text{eff}}^{\text{dd}} \rightarrow 0, \\ (g_{\text{eff}}^{\text{dd}})^{5/2} \mathcal{M}_5(1/\epsilon_{\text{eff}}^{\text{dd}}) = (g_{\text{eff}})^{5/2} \mathcal{Q}_5(\epsilon_{\text{eff}}^{\text{dd}}), & g_{\text{eff}} > 0, \end{cases} \quad (6)$$

showing this expression reduces to known results for the binary contact [2] and single component dipolar [10] condensates, respectively (see [10] for the definition of \mathcal{Q}_5 - note \mathcal{M}_5 is useful because it is well-defined for $\epsilon_{\text{eff}}^{\text{dd}} \leq 0$).

Within the SSA, a useful variational description is furnished by making a Gaussian ansatz for the condensate wavefunction $\psi_i^{\text{var}} = \sqrt{8N_i/\pi^{3/2}\sigma_\rho^2\sigma_z} e^{-2(\rho^2/\sigma_\rho^2 + z^2/\sigma_z^2)}$, where σ_ρ and σ_z are the variational width parameters. Variational solutions are found by minimising the variational energy³

$$\begin{aligned} \frac{E_i}{N_i} = & \frac{\hbar^2}{m} \left(\frac{2}{\sigma_\rho^2} + \frac{1}{\sigma_z^2} \right) + \frac{4N_i \left[g_{\text{eff}} - g_{\text{eff}}^{\text{dd}} f\left(\frac{\sigma_\rho}{\sigma_z}\right) \right]}{(2\pi)^{3/2} \sigma_\rho^2 \sigma_z} \\ & + \frac{2\gamma_{\text{QF}}}{5} \left(\frac{16N_i}{5\pi^{3/2} \sigma_\rho^2 \sigma_z} \right)^{3/2}, \end{aligned} \quad (7)$$

where $f(x) = \frac{1+2x^2}{1-x^2} - \frac{3x^2 \tanh^{-1} \sqrt{1-x^2}}{(1-x^2)^{3/2}}$.

In free-space (i.e. $V = 0$) self-bound droplets are stable ground states where their energy is negative, otherwise they are unstable to evaporating to the trivial solution ($\psi_i \rightarrow 0$). In Fig. 1(a) we present a phase diagram obtained from the variational theory with $E_i = 0$ taken to define the stable droplet boundary. This shows that, for a given atom number, a stable droplet will occur when the intra-species scattering length is below some threshold value. This threshold tends to decrease with increasing a_{12} , as the inter-species repulsion competes against the attractive DDIs. For reference the self-binding boundary for a single component droplet⁴ [12] is also indicated. This shows that the BMG droplets can be stable in regimes where each component could not form a stable droplet by itself. In the inset we present the phase diagram rescaled to the effective parameters and show that the boundaries approximately collapse to a single curve.

In Fig. 1(b1) we show an example of a miscible droplet obtained by solving the eGPE, in a regime where both components have identical wavefunctions. In this case the full eGPE is equivalent to the SSA eGPE [see Eqs. (1) and (4)]. As the value of a_{12} is lowered, the two components become immiscible and phase-separate – thus the SSA is no longer applicable. The two separated components orient in a head-to-tail configuration to minimise the DDI energy [see Fig. 1(b2)].

For the balanced system in the miscible regime (where the SSA applies) the DDIs are identical within and between the components. Thus immiscibility is determined by the

² $\ln|1-x|$ for $x \geq -2$ and $\mathcal{M}_5(x) = 0$ otherwise.

³ Obtained from the energy functional associated with operator in Eq. (4), and has similar form to the single component dipolar result of Ref. [11].

⁴ I.e. for a single component system with parameters N_i , a_{ii} and a_{ii}^{dd} .

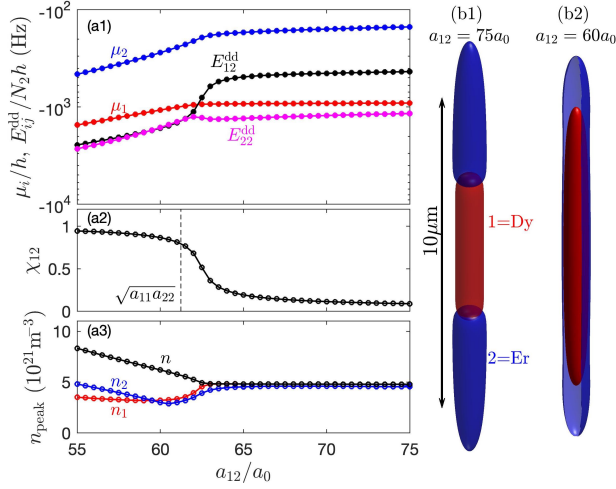


FIG. 2. Immiscibility transition of a free-space BMG droplet comprised of $N_1 = 5 \times 10^3$ Dy atoms and $N_2 = 10^4$ Er atoms. (a1)-(a3) Chemical potentials, DDI energies, component overlap and peak densities as the interspecies scattering length is changed across the immiscibility transition. (b1), (b2) Density isosurfaces at $5 \times 10^{20}/\text{m}^3$ of the ground states at labeled a_{12} values [component 2 is cut away in (b2) to reveal component 1]. Other parameters: $\{a_{11}, a_{22}, a_{11}^{\text{dd}}, a_{22}^{\text{dd}}\} = \{75, 50, 130.8, 65.5\}a_0$, and $m = 165u$.

short-ranged interactions with the transition occurring when $a_{12} = \sqrt{a_{11}a_{22}}$ [13]. This allows us determine the regions (shaded) of the phase diagram where the BMG droplets are miscible. In Fig. 1(c) and (d) we show the peak densities and the overlap $\chi_{12} \equiv \frac{1}{\sqrt{N_1 N_2}} \int dx \psi_1^* \psi_2$ (quantifying miscibility) as the transition is crossed by varying a_{ii} for $a_{12} = 90a_0$.

We have calculated stationary droplet states of the full eGPE and the SSA eGPE to determine the self-binding phase boundary. These results are generally in good agreement with, although lie slightly above, the variational boundaries. An exception is for $a_{12} = 90a_0$ and $N_1 \lesssim 3 \times 10^3$. In this region the variational boundary is below the immiscibility line, and the droplets are immiscible at the boundary. As such both the variational and SSA eGPE are inapplicable, and the full eGPE predicts a significantly higher phase boundary. Here the self-binding line is similar to the single droplet case – expected since the droplets components have spatially separated – but it is shifted upwards (relative to the single-droplet boundary) due to the stabilizing attractive DDI between the components.

Quantum droplets in an imbalanced BMG - Our formalism applies to the general imbalanced case where the atom number and intra-species interactions are different. In Fig. 2 we consider the ground state droplet properties of Dy-Er BMG as the inter-species scattering length is ramped through the immiscibility transition. These solutions are obtained by numerically solving for the ground states of the full eGPE.

The chemical potential μ_i is the energy required to add a particle of component- i and provides a useful characterization of the system. The values of μ_i in Fig. 2(a1) are negative, indicating that both components are self-bound. In the regime we examine, μ_1 (for Dy) is less than μ_2 (for Er). We also see that μ_i increases with increasing a_{12} when the system is miscible

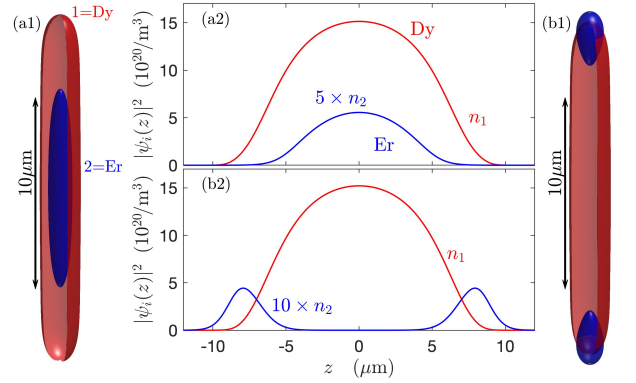


FIG. 3. Er condensate confined by a Dy droplet in free-space. (a1,b1) Dy (red) and Er (blue) density isosurfaces at $2 \times 10^{19}/\text{m}^3$, and (a2,b2) the respective density on the z -axis. In (a) $a_{12} = 65a_0$ and in (b) $a_{12} = 70a_0$. Other parameters: $N_1 = 10^4$, $N_2 = 500$, $\{a_{11}, a_{22}, a_{11}^{\text{dd}}, a_{22}^{\text{dd}}\} = \{90, 80, 130.8, 65.5\}a_0$, and $m = 165u$.

[i.e. where $\chi_{12} \sim 1$, see (a2)], since a_{12} makes an important contribution to the energy when the components spatially overlap. When the system transitions to being immiscible, the chemical potentials become almost independent of a_{12} . However, the DDIs between the components still play an important role. To quantify this we show the inter- and intra-species DDI energies $E_{ij}^{\text{dd}} = \frac{1}{2} g_{ij}^{\text{dd}} \int dx n_i \Phi_j$ in Fig. 2(a1). We see that, even when the system is immiscible, $|E_{12}^{\text{dd}}/N_2| > |\mu_2|$, i.e. the inter-species DDI energy per particle is larger (in magnitude) than the Er chemical potential. This emphasises the often dominant role of long-ranged inter-component interactions in this system.

The Dy density is slightly higher than the Er density in the immiscible regime [$a_{12} \gtrsim 60a_0$ in Fig. 2(a3)], and the phase-separated droplet organizes to have the Dy component at the center with Er component above and below [see Fig. 2(b1)]. By increasing a_{11} we find similar behavior to Fig. 2, but the Dy density decreases (in the immiscible regime) and the Er component moves to the center of the droplet.

In Fig. 3 we consider a more strongly imbalanced case of 10^4 Dy atoms and 500 Er atoms. Taking $a_{11} = 90a_0$ ($< a_{11}^{\text{dd}}$) for Dy, it is in a regime where it forms a self-bound droplet by itself. For Er $a_{22} = 80a_0$ ($> a_{22}^{\text{dd}}$) so that its overall intra-species interactions are contact dominated and repulsive (i.e. it will not bind into a droplet) and can be considered as a regular dipolar condensate that would evaporate in free-space. For the combined system, the inter-species interactions allow the Dy droplet to bind the Er atoms. For the case in Fig. 3(a1,a2) the components are miscible and the Er atoms sit in the middle of the Dy droplet, while the case in Fig. 3(b1,b2) (with higher a_{12}) is immiscible, and the Er atoms are instead confined to the effective potential minima at the top and bottom of the Dy droplet arising from the attractive DDIs. In both cases the Dy component is only weakly affected by the Er component which is more than an order of magnitude less dense.

Preparation dynamics of BMG droplets - Here we simulate a procedure to prepare a BMG droplet, starting from a trapped condensate in the miscible regime, and then reducing

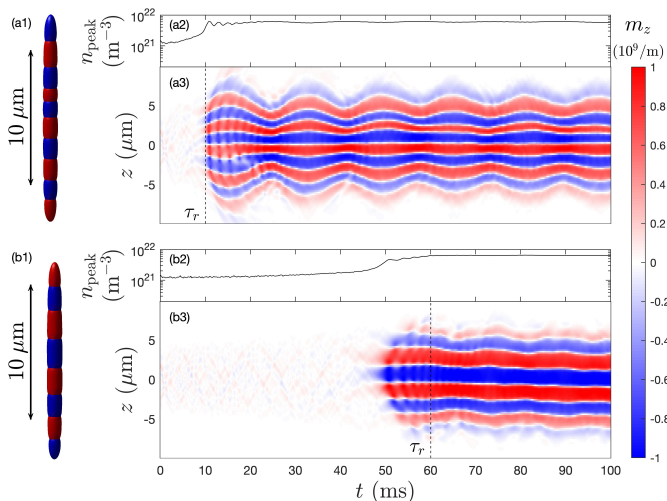


FIG. 4. Preparation of BMG droplets from an initial miscible Dy-Dy condensate. (a1)-(a3) Results from a $\tau_r = 10$ ms ramp. (a1) $10^{20}/\text{m}^3$ density isosurfaces of component 1 (red) and 2 (blue) at $t = 100$ ms. Evolution of (a2) peak total density n_{peak} and (a3) pseudo-spin density m_z . (b1)-(b3) Similar analysis for a $\tau_r = 60$ ms ramp. Initial and final values for the intra-species scattering lengths are $a_{ii} = 110a_0$ and $a_{ii}^f = 80a_0$, respectively. The initial harmonic confinement is $V = \frac{1}{2}m \sum_{\nu} \omega_{\nu}^2 x_{\nu}^2$, with $\omega_{x,y}/2\pi = 250\text{Hz}$, and $\omega_z/2\pi = 125\text{Hz}$. Other parameters: $N_i = 5 \times 10^3$, $a_{ii}^{\text{dd}} = 130.8a_0$, $a_{12} = 90a_0$ and $m = 163.9u$.

the scattering lengths into the droplet regime while removing the trap potential (cf. [7, 14]). We use the time-dependent eGPE $i\hbar\psi_i = \mathcal{L}_i\psi_i$ from an initial state corresponding to a harmonically trapped condensate with noise added to mimic vacuum fluctuations [15], following the procedure described in Ref. [16] (also see [17, 18]). At $t = 0$ we ramp into the droplet regime over a time period of τ_r , by linearly reducing the intra-species scattering lengths a_{ii} to a final value a_{ii}^f , and linearly reducing the trap frequencies to zero. These parameters are then held constant for the remainder of the simulation.

For a_{ii}^f in the range $(90a_0, 103a_0)$ the free-space ground state is a miscible BMG droplet (cf. Fig. 1). Simulations of this case (not shown) successfully generate a self-bound droplet with collective oscillations excited by the finite ramp time (similar to the single component simulations in Ref. [12]). The droplet produced lasts for the duration of

our simulations ($\gtrsim 100$ ms) without any noticeable decay. The inclusion of three-body loss would limit the droplet lifetime.

For $a_{ii}^f \lesssim 90a_0$ the ground state droplet is immiscible with two domains [cf. Fig. 1(b2)]. We show results simulating the evolution in this regime for $\tau_r = 10$ ms and 60 ms in Fig. 4. The droplet produced by the ramp has a greater number of domains, with a nearly periodic spatial pattern. We characterize the domain formation and its evolution with the (pseudo)-spin density $m_z(z) \equiv \int dx dy (|\psi_1|^2 - |\psi_2|^2)$ in Fig. 4(a3) and (b3). This observable reveals the domains appearing near the conclusion of the ramp, and the breathing-mode-like collective excitation of these domains along the z axis. Note that we do not observe any merging or decay of the domains once they form even under these strong collective dynamics, demonstrating that these structures are robust. For the slower ramp we find that fewer domains are produced. This τ_r -dependence is similar to that found in studies of the domain formation in the immiscibility transition of a binary condensate [19, 20], which was described using the Kibble-Zurek mechanism. This suggests that the additional domains we observe are defects arising from non-adiabatically crossing the phase transition.

Conclusions and outlook - We have developed a theory for a new category of quantum droplet that exhibits the rich behavior of binary fluids. Using this theory we have characterized a droplet phase diagram and the properties of miscible and immiscible droplets. We have shown that a single magnetic droplet can be used to bind a magnetic condensate, and thus potentially even individual magnetic atoms. This test tube-like behavior has similarities to helium nanodroplets, which act as quantum solvents to attach other chemical species, e.g. for mK spectroscopy [21]. We have also considered the dynamics of forming a BMG droplet from an initial trapped condensate in the miscible regime, showing that an interaction and trap ramp can be used to prepare self-bound droplets on the typical time scales available to experiments. Crossing the immiscibility transition at a finite rate leads to additional domains being created compared to the ground state case. Pathways to produce a droplet closer to the ground state case include (i) using a slower ramp, (ii) ramping down from an immiscible condensate (i.e. already having several domains), or (iii) directly evaporatively cooling into the droplet regime (cf. Ref. [17]).

Acknowledgments - We acknowledge support from the Marsden Fund of the Royal Society of New Zealand and useful discussions with Au-Chen Lee.

-
- [1] Aurel Bulgac, “Dilute quantum droplets,” *Phys. Rev. Lett.* **89**, 050402 (2002).
 [2] D. S. Petrov, “Quantum mechanical stabilization of a collapsing Bose-Bose mixture,” *Phys. Rev. Lett.* **115**, 155302 (2015).
 [3] C. R. Cabrera, L. Tanzi, J. Sanz, B. Naylor, P. Thomas, P. Cheiney, and L. Tarruell, “Quantum liquid droplets in a mixture of Bose-Einstein condensates,” *Science* **359**, 301–304 (2018).
 [4] G. Semeghini, G. Ferioli, L. Masi, C. Mazzinghi, L. Wolswijk,

- F. Minardi, M. Modugno, G. Modugno, M. Inguscio, and M. Fattori, “Self-bound quantum droplets of atomic mixtures in free space,” *Phys. Rev. Lett.* **120**, 235301 (2018).
 [5] C. D’Errico, A. Burchianti, M. Prevedelli, L. Salasnich, F. Ancilotto, M. Modugno, F. Minardi, and C. Fort, “Observation of quantum droplets in a heteronuclear bosonic mixture,” *Phys. Rev. Research* **1**, 033155 (2019).
 [6] Igor Ferrier-Barbut, Holger Kadau, Matthias Schmitt, Matthias Wenzel, and Tilman Pfau, “Observation of quantum droplets

- in a strongly dipolar Bose gas,” *Phys. Rev. Lett.* **116**, 215301 (2016).
- [7] L. Chomaz, S. Baier, D. Petter, M. J. Mark, F. Wächtler, L. Santos, and F. Ferlaino, “Quantum-fluctuation-driven crossover from a dilute Bose-Einstein condensate to a macrodroplet in a dipolar quantum fluid,” *Phys. Rev. X* **6**, 041039 (2016).
- [8] A. Trautmann, P. Ilzhöfer, G. Durastante, C. Politi, M. Sohmen, M. J. Mark, and F. Ferlaino, “Dipolar quantum mixtures of erbium and dysprosium atoms,” *Phys. Rev. Lett.* **121**, 213601 (2018).
- [9] Hui Hu and Xia-Ji Liu, “Consistent theory of self-bound quantum droplets with bosonic pairing,” [arXiv:2005.08581](https://arxiv.org/abs/2005.08581).
- [10] Aristeu R. P. Lima and Axel Pelster, “Quantum fluctuations in dipolar Bose gases,” *Phys. Rev. A* **84**, 041604 (2011).
- [11] R. N. Bisset, R. M. Wilson, D. Baillie, and P. B. Blakie, “Ground-state phase diagram of a dipolar condensate with quantum fluctuations,” *Phys. Rev. A* **94**, 033619 (2016).
- [12] D. Baillie, R. M. Wilson, R. N. Bisset, and P. B. Blakie, “Self-bound dipolar droplet: A localized matter wave in free space,” *Phys. Rev. A* **94**, 021602(R) (2016).
- [13] V.P. Mineev, “The theory of the solution of two near-ideal Bose gases,” *Zh. Eksp. Teor. Fiz.* **67**, 263 (1974).
- [14] Matthias Schmitt, Matthias Wenzel, Fabian Böttcher, Igor Ferrier-Barbut, and Tilman Pfau, “Self-bound droplets of a dilute magnetic quantum liquid,” *Nature* **539**, 259–262 (2016).
- [15] P. B. Blakie, A. S. Bradley, M. J. Davis, R. J. Ballagh, and C. W. Gardiner, “Dynamics and statistical mechanics of ultracold Bose gases using c-field techniques,” *Adv. Phys.* **57**, 363 (2008).
- [16] R. N. Bisset and P. B. Blakie, “Crystallization of a dilute atomic dipolar condensate,” *Phys. Rev. A* **92**, 061603 (2015).
- [17] L. Chomaz, D. Petter, P. Ilzhöfer, G. Natale, A. Trautmann, C. Politi, G. Durastante, R. M. W. van Bijnen, A. Patscheider, M. Sohmen, M. J. Mark, and F. Ferlaino, “Long-lived and transient supersolid behaviors in dipolar quantum gases,” *Phys. Rev. X* **9**, 021012 (2019).
- [18] G. Natale, R. M. W. van Bijnen, A. Patscheider, D. Petter, M. J. Mark, L. Chomaz, and F. Ferlaino, “Excitation spectrum of a trapped dipolar supersolid and its experimental evidence,” *Phys. Rev. Lett.* **123**, 050402 (2019).
- [19] Jacopo Sabbatini, Wojciech H. Zurek, and Matthew J. Davis, “Phase separation and pattern formation in a binary Bose-Einstein condensate,” *Phys. Rev. Lett.* **107**, 230402 (2011).
- [20] E. Nicklas, M. Karl, M. Höfer, A. Johnson, W. Muessel, H. Strobel, J. Tomkovič, T. Gasenzer, and M. K. Oberthaler, “Observation of scaling in the dynamics of a strongly quenched quantum gas,” *Phys. Rev. Lett.* **115**, 245301 (2015).
- [21] Frank Stienkemeier and Kevin K Lehmann, “Spectroscopy and dynamics in helium nanodroplets,” *J. Phys. B* **39**, R127 (2006).
- [22] Gianmaria Durastante, Claudia Politi, Maximilian Sohmen, Philipp Ilzhöfer, Manfred J. Mark, Matthew A. Norcia, and Francesca Ferlaino, “Feshbach resonances in an erbium-dysprosium dipolar mixture,” [arXiv:2006.06456](https://arxiv.org/abs/2006.06456).